Synthesis, Characterization and Biological Activity of Cadmium (II) Complex of Hydrazone Moiety

Samar A. Aly[1]*, Safaa S. Hassan[2], Safinaz A. Farfour[1], Ehab M. Abdalla[3*] and Tasneem A. Abdel-hady[1]

[1]Department of Environmental Biotechnology, Genetic Engineering and Biotechnology Research Institute, University of Sadat City 32958, Egypt.
[2]Chemistry Department, Faculty of Science, Cairo University, Giza 12613, Egypt.
[3]Chemistry Department, Faculty of Science, New Valley University, Alkharga 72511, Egypt.

DOI: 10.21608/rjab.2024.312873.1055

Corresponding author1: Prof. Samar A. Aly
E-mail: **samar.mostafa@gebri.usc.edu.eg**
Tel: **+201063936729**
Corresponding author2: Dr. Ehab M. Abdalla
E-mail: **Ehababdalla99@sci.nvu.edu.eg**
Tel: **+201008275126**

ABSTRACT:

With the aid of hydrazone moiety, a novel Cd (II) chelate with 2-[(4-methylphenyl) amino]-*N*'-[(*Z*)-thiophen-2-ylmethylidene] acetohydrazide (H_2L) was created and reported. These novel chemicals' structural makeup was clarified through the utilization of spectroscopic and analytical methods. The chelates were molded with a molar ratio of 1:1 M:L and the formula $[Cd(H_2L)Cl_2]$. Cd(II) complex of the biological activity ligand is investigated. Theoretical measurements supported the proposed generic formula for the $[Cd(H_2L)Cl_2]$ complex. The compound's anticancer and antibacterial properties were evaluated using cisplatin, gentamicin, and ampicillin as standards. It was found that the Cd^{2+} complex was more effective against two cancer cell lines and several bacterial strains than it was against ligand. The results showed that the compound's activities were: Cd (II) complex > H_2L, with Cd (II) complex exhibiting the maximum activity. By examining the binding between the complex and Penicillin-binding protein PBP, which is primarily thought of as the production of the cell wall through its transglycosylation and transpeptidation, a molecular docking study was carried out to support the microbial inhibition growth.

Keywords: Complex, Antibacterial, Anticancer, Molecular Docking

1. INTRODUCTION

A significant family of compounds with a wide range of medicinal chemistry uses are hydrazone derivatives (Aly *et al*., 2021). These applications result from of extent of their pharmacokinetic properties (Rizk *et al*., 2022) (Popiołek *et al*., 2018; Aneja *et al*., 2019; El-saied *et al*., 2020; Katariya *et al*., 2020), especially their importance in drug-identification programs (Kumar *et al*., 2009; Eswaran *et al*., 2010). Numerous investigations have demonstrated the extensive spectrum of biological properties exhibited by the complexes of the derivatives of hydrazone and carbamazehyde. (Sepay and Dey, 2014; Parveen *et al*., 2018; Naveen *et al*., 2020; Zülfikaroğlu *et al*., 2020), as well as antimycobacterial (Mandewale *et al*., 2017; Manohar *et al*., 2018; Yousefi *et al*., 2019; Babahan *et al*., 2020), anticancer (Ekennia *et al*., 2018; Özbek *et al*., 2019; Khan *et al*., 2020). Additionally, they are crucial in the treatment of Alzheimer's (Haghighijoo *et al*., 2017; Parlar *et al*., 2019). N'-((5-hydroxy-4-oxo-4H-pyran-3-yl)methylene)-2-(p-

tolylamino)acetohydrazide (H_2L) has been used to produce a new series of Zr^{4+}, V^{4+}, Ru^{3+}, and Cd^{2+}complexes (Elganzory *et al*., 2022b). To clarify the structural makeup of novel compounds, several techniques were used. Furthermore, the antibacterial and anticancer properties of the ligand and its compound properties were investigated. It was discovered that the Cd^{2+} chelate acquired likely the greatest antibacterial activity against bacterial species when ampicillin and gentamicin were given as regular medications, with the Ru (III) complex coming in second. The compounds showed intriguing anticancer potential when tested against the breast cancer cell line MCF-7. The novel compounds' cytotoxicity has been arranged in the following order: Complex Ru(III) > Complex Ru^{3+} chelate > Cd^{2+} chelate > Zr^{4+} chelate > V^{4+} chelate > H_2L The ribosyltransferase active site underwent successful molecular docking. A possible therapeutic inhibitor for NUDT5 is found using structure-based molecular docking. This paper presents the synthesis, characterization, and bioactivities of the Cd2+complex with a ligand generated from derivatives of hydrazone.

2. MATERIAL AND METHODES

The materials, tools and techniques for applying and verifying structural integrity are covered in great depth in the supplemental file (**Section S1**). (**Part S2**): antimicrobial process (Hare, 1968; Abdalla *et al*., 2020a; Aly *et al*., 2023).

2.1. Synthesis of Cd (II) complex

The Cd^{2+} complex was prepared by magnetically stirring a solution of 0.002 moles of $CdCl_2$. $2H_2O$ in ethanol for five to nine hours while adding 0.002 moles of the relevant ligands to 50 milliliters of EtOH (Abo-Rehab *et al*.; Abdalla and Abd-Allah, 2022). The resultant particles were removed by filtering, repeatedly cleaned with EtOH, and vacuum-dried on P_4O_{10} (**Structures 1)**.

3. RESULTS AND DISCUSSION

3.1. Characteristics of Compounds

3.1.1. The physical-chemical characteristics

The color of the Cd (II) complex does not change when exposed to air or moisture. The complex's analytical results are in agreement with the suggested formulae for molecules and validate the formation of a 1:1 (M:L) complex, **structures 1**. The molar conductivity value of Cd (II) complex was 10 $\Omega^{-1}cm^2mol^{-1}$ in DMF solution. Their complex values show that there is no electrolysis involved (Table 1). (Nunes *et al*., 2020; Sardaru *et al*., 2021).

3.2 FT-IR Spectra of Ligand and Cd (II) Complex

Four bands, compatible to υ(N-H), υ (C=O), υ (C=N), and υ (C-S), are noticeable at 3410-3096, 1705, 1612, and 702 cm^{-1} in the infrared spectrum (Table 2 and Figure 1). Strong bands are seen at 3402, 1571, 1600, 1595, 703, 531, and 453 cm^{-1} in the infrared spectra of the Cd^{2+} complex Figure 2, that are credited to υ(N-H), υ (C=N), υ (C=O), and υ (C=N). The previous shift demonstrated the sharing of the C=O group in chelation, and it was accompanied by the emergence of additional bands at (531 and 453) cm^{-1}, which corresponded to ν(M—O) and ν(M—N) (Abdel-Rahman *et al*., 2023; Alshater *et al*., 2023; Abo-Rehab *et al*., 2024). The prior theory that nitrogen azomethine and carbonyl oxygen would be involved in the chelation of metal was validated (Gaber *et al*., 2019; Elganzory *et al*., 2022a) with the formation of a hexagonal ring using the carbaldehyde molecule (Aly and Fathalla, 2020).

3.3. Electronic spectra

The UV–V spectra of the H_2L and Cd (II) chelate combination were measured between 200 and 800 nm in DMSO at room temperature. Two absorption bands were visible in the ultraviolet portion of the ligand's absorption spectra (Liu *et al*., 2013). At λ_{max} = 0.0000339 cm, the initial high-intensity bands were detected, while at λ_{max}

= 0.0000389 cm, the second low-intensity bands were found. The azomethine group's (n-π*) transition is linked to the two bands (Abdalla *et al.*, 2020b). The azomethine group is linked to the (n-π*) transition, which was observed in the Cd (II) complex's electronic spectrum around 0.0000337 and 0.0000371 cm.

3.4. ESI-MS spectra

Molecular peak at 456.67 amu is detectable in the mass spectrum of the Cd^{2+} complex. Figure 3 illustrates how well these results match the predicted chemical formulas for the Cd^{2+} complex.

3.5. Thermogravimetric analysis

Figure 4 illustrates the thermal stability pattern of the synthesized cadmium chelate (TGA curve) that was obtained in a nitrogen environment, with a heating rate of 10 ºC min/1 from ambient temperature to 800 ºC. The biggest fragment of the organic ligand and the two chloride ligands broke down in a rapid step at 272.2 ºC, which is significant for the breakdown of the cadmium complex. At 480.7 ºC, the ligand's breakdown was complete, resulting in a final mass loss of 71.80% (observed, calculated = 71.90%). The ultimate residual form is cadmium oxide, which has a residual percentage of 28.20% (calculated = 28.11%) compared to 28.20% observed.

3.6. DFT Calculation:

Tables 3&4 and (Figures 5, and 6) discussed the geometric optimization and molecular characteristics of H_2L and its produced Cd^{2+} chelate. The optical and electric properties are significantly influenced by frontier molecular orbitals (FMOs), which are expressed in the higher occupied molecular orbital (HOMO) and the lower unoccupied molecular orbital (LUMO). The terms HOMO and LUMO denote the ability to donate and take electrons, respectively. In Figure 6, the molecular surfaces are made clear. A molecule's chemical reactivity, optical polarizability, and chemical hardness and softness can all be described using the frontier orbital gap. The definitions of ionization energy (I) and electron affinity (A) are $I = -E_{HOMO}$ and $A = -E_{LUMO}$, respectively. The HOMO-LUMO gap (ΔE) can be used to determine the polarity of a molecule. A larger ΔE indicates a tougher molecule, while a smaller ΔE indicates a softer molecule. Because the soft molecule requires less energy to excite than the hard molecule, it is more polarizable. One can compute these molecular characteristics in the following way:

Chemical potential (μ), which is equal to $-(I + A)/2$, softness $(S) = 1/2\eta$, and hardness $(\eta) = (I-A)/2$.

As stated in Table 4, modifications to the bond lengths and angles of complexes upon complexation with Cd (II) ions are made to maximize the values of the tetrahedral geometry. Some bonds are elongated as R(N4-N5) and others are reduced as R(C1-N4) **to** be suitable for the coordination with the cadmium ion. Similar behavior was observed in the case of bond angles, the angles are changed as seen in Table 4 to maximize the desired structure of the investigated complex. The value of dipole moments indicates that the ligand's polarity increased following complexation.

3.7. Biological applications

3.7.1. Antibacterial bioassay

It has been discovered that some prescription medications are more effective against Gram-positive bacteria than Gram-negative bacteria. Using the agar diffusion method, the antibacterial activity of the ligand and Cd (II) complex against several microbial species was evaluated in this study. The measured bactericidal activity of Cd (II) and ligand is listed in Table 5 and Figure 7 (Reedijk and Bouwman, 1999). The ligand's action against a number of bacterial strains increased when it chelated with Cd (II). The complex exhibit enhanced antibacterial activity due to delocalization of electrons throughout the entire chelate ring system, which is caused through the donor (N and O) atoms of the ligand partially

sharing the positive charge of the metal ion. Given that the complex's geometric structure, the kind of metal ion, ligand donor atoms, the total complex charge, and the chelating effect of the H_2L all disturb the biological activity of metal compounds (Ispir, 2009). Against the examined microorganisms, particularly B. cereus and E. coli, the cadium complex demonstrates a strong antibacterial activity. To bolster the microbial growth suppression, a theoretical investigation was performed to explore the complex's affinity to Penicillin-binding protein PBP. PBP is mainly considered as a precursor for transglycosylation and transpeptidation, which are processes involved in the manufacture of cell walls. Antibiotic-resistant pathogenic bacterial strains may be produced as a result of PBP replacement. The mutant-type PBP5 structure (PDB ID: 1NJ4) was obtained from the Protein Data Bank. The interaction analyses of the complex are shown in Figure 10. -9.00 kcal/mol was the scoring energy value used for the interaction. The active amino acids are Met 89 and Asp 105, which demonstrate interactions of Metal Contact and Sidechain acceptor, respectively (Pisano *et al*., 2019; El-Etrawy and Sherbiny, 2021).

3.7.2 Cytotoxicity

Applying the MTT test assay, the compounds' in vitro cytotoxicity against the human MCF7 breast cancer cell line was assessed. Mitochondrial dehydrogenase activity, a measure of cell viability, is quantified using the MTT assay. The absorbance values were assessed using non-linear regression approaches to limit the IC_{50} values for the chemicals being studied in the two cancer cell lines (Abdalla *et al*., 2020a; Al-Farhan *et al*., 2021; Alshater *et al*., 2023). The cytotoxicity results for MCF7 at dosages of 31.25, 62.5, 125, 250, 500, and 1000 µg/ml for H_2L and Cd^{2+} combination is exposed in Table 6 and Figure 8. By comparing the IC_{50} values of H_2L and Cd^{2+} complex with cisplatin as the standard reference, when we analyzed the IC_{50} values for H_2L and Cd^{2+} complex, we found that, in the existence of MCF7, the activity proceeded as follows: cisplatin > Cd (II) complex > Ligand.

3.7.3 Molecular Docking Study

H_2L and Cd^{2+} complex exhibits potent antibacterial effect against the investigated microorganisms specially *E. coli* and *B. cereus*. A molecular docking investigation was carried out to support the microbial inhibition growth by investigating the binding between the ligand and its complex with Penicillin-binding protein PBP that is majorly considered the precursor for the biosynthesis of cell wall biosynthesis by its transglycosylation and transpeptidation. The mutant-type PBP5 structure was downloaded (PDB ID: 1NJ4) from the Protein Data Bank. Interaction analyses of the complex was seen in (Figure 7). The interaction was performed with scoring energy value -3.79 (1.28) and -7.20 (1.96) kcal/mol relative to the ligand and its Cd^{2+} complex, respectively. Asp 113 played a key role as the primary amino acid when studying a ligand that showed two different types of interactions: sidechain acceptor and backbone donor. Met 89 is involved in a metal contact interaction type within the complex (Pisano *et al*., 2019; El-Etrawy and Sherbiny, 2021).

4. CONCLUSION

This work used a variety of spectroscopic and structural techniques to construct a unique Cd^{2+} complex and completely characterized it. They used a range of bacterial strains and human MCF7 breast cancer cell lines to assess their biological activities. The study revealed that the Cd^{2+} complex outperformed the ligand against two cancer cell lines and several bacterial strains. Data from thermal, FTIR, molar conductivity, and elemental analysis revealed that the Cd^{2+} chelate was molded using the formula $[Cd(H_2L)Cl_2]$ with a molar percentage of 1:1 M:L.

5. REFERENCES

Abdalla, E.M., and Abd-Allah, M. (2022). Synthesis, Characterization,

Antimicrobial/Antitumor Activity of Binary and Ternary Neodymium (III) Complex with 2, 2'-((1E, 1'E)-(ethane-1, 2-diylbis (azaneylylidene)) bis (methaneylylidene)) diphenol and Imidazole. *Egyptian Journal of Chemistry* 65**,** 735-744.

Abdalla, E.M., Abdel Rahman, L.H., Abdelhamid, A.A., Shehata, M.R., Alothman, A.A., and Nafady, A. (2020a). Synthesis, characterization, theoretical studies, and antimicrobial/antitumor potencies of salen and salen/imidazole complexes of Co (II), Ni (II), Cu (II), Cd (II), Al (III) and La (III). *Appl. Organomet. Chem.* 34**,** e5912.

Abdalla, E.M., Abdel Rahman, L.H., Abdelhamid, A.A., Shehata, M.R., Alothman, A.A., and Nafady, A. (2020b). Synthesis, characterization, theoretical studies, and antimicrobial/antitumor potencies of salen and salen/imidazole complexes of Co (II), Ni (II), Cu (II), Cd (II), Al (III) and La (III). *Applied Organometallic Chemistry* 34**,** e5912.

Abdel-Rahman, L.H., Abdelghani, A.A., Alobaid, A.A., El-Ezz, D.A., Warad, I., Shehata, M.R., and Abdalla, E.M. (2023). Novel Bromo and methoxy substituted Schiff base complexes of Mn (II), Fe (III), and Cr (III) for anticancer, antimicrobial, docking, and ADMET studies. *Sci. Rep.* 13**,** 3199.

Abo-Rehab, R.S., Aboul Kasim, E., Farhan, N., and Abdalla, E.M. (2024). Physicochemical studies of Cu (II) complex and antibacterial, anticancer activities bearing N, O-chelated Schiff base ligand. *New Valley University Journal of Basic and Applied Sciences* 2**,** 8-17.

Abo-Rehab, R.S., Kasim, E.A., Farhan, N., Tolba, M.S., Shehata, M.R., and Abdalla, E.M. Synthesis, characterization, anticancer, antibacterial, antioxidant, DFT, and molecular docking of novel La (III), Ce (III), Nd (III), and Dy (III) lanthanide complexes with Schiff base derived from 2-aminobenzothiazole and coumarin. *Applied Organometallic Chemistry***,** e7622.

Al-Farhan, B.S., Basha, M.T., Abdel Rahman, L.H., El-Saghier, A.M., Abou El-Ezz, D., Marzouk, A.A., Shehata, M.R., and Abdalla, E.M. (2021). Synthesis, dft calculations, antiproliferative, bactericidal activity and molecular docking of novel mixed-ligand salen/8-hydroxyquinoline metal complexes. *Molecules* 26**,** 4725.

Alshater, H., Al-Sulami, A.I., Aly, S.A., Abdalla, E.M., Sakr, M.A., and Hassan, S.S. (2023). Antitumor and antibacterial activity of Ni (II), Cu (II), Ag (I), and Hg (II) complexes with ligand derived from thiosemicarbazones: characterization and theoretical studies. *Molecules* 28**,** 2590.

Aly, S.A., Eldourghamy, A., El-Fiky, B.A., Megahed, A.A., El-Sayed, W.A., Abdalla, E.M., and Elganzory, H.H. (2023). Synthesis, spectroscopic characterization, thermal studies, and molecular docking of novel Cr (III), Fe (III), and Co (II) complexes based on Schiff base: In vitro antibacterial and antitumor activities. *Journal of Applied Pharmaceutical Science* 13**,** 196-210.

Aly, S.A., Elganzory, H.H., Mahross, M.H., and Abdalla, E.M. (2021). Quantum chemical studies and effect of gamma irradiation on the spectral, thermal, X-ray diffraction and DNA interaction with Pd (II), Cu (I), and Cd (II) of hydrazone derivatives. *Applied Organometallic Chemistry* 25**,** e6153.

Aneja, B., Khan, N.S., Khan, P., Queen, A., Hussain, A., Rehman, M.T., Alajmi, M.F., El-Seedi, H.R., Ali, S., and Hassan, M.I. (2019). Design and development of Isatin-triazole hydrazones as potential inhibitors of microtubule affinity-regulating kinase 4 for the therapeutic management of cell proliferation and metastasis. *European Journal of Medicinal Chemistry* 163**,** 840-852.

Babahan, I., Özmen, A., Aksel, M., Bilgin, M.D., Gumusada, R., Gunay, M.E., and Eyduran, F. (2020). A novel bidentate ligand containing oxime, hydrazone and

indole moieties and its BF2+ bridged transition metal complexes and their efficiency against prostate and breast cancer cells. *Applied Organometallic Chemistry* 34**,** e5632.

Ekennia, A.C., Osowole, A.A., Onwudiwe, D.C., Babahan, I., Ibeji, C.U., Okafor, S.N., and Ujam, O.T. (2018). Synthesis, characterization, molecular docking, biological activity and density functional theory studies of novel 1, 4-naphthoquinone derivatives and Pd (II), Ni (II) and Co (II) complexes. *Applied Organometallic Chemistry* 32**,** e4310.

El-Etrawy, A.-a.S., and Sherbiny, F.F. (2021). Design, synthesis, biological assessment and molecular docking studies of some new 2-Thioxo-2, 3-dihydropyrimidin-4 (1H)-ones as potential anticancer and antibacterial agents. *Journal of Molecular Structure* 1225**,** 129014.

El-Saied, F.A., Shakdofa, M.M., Al-Hakimi, A.N., and Shakdofa, A.M. (2020). Transition metal complexes derived from N′-(4-fluorobenzylidene)-2-(quinolin-2-yloxy) acetohydrazide: Synthesis, structural characterization, and biocidal evaluation. *Applied Organometallic Chemistry* 34**,** e5898.

Elganzory, H.H., Hassan, S.S., Aly, S.A., and Abdalla, E.M. (2022a). Synthesis, characterization, PXRD studies, theoretical calculation, and antitumor potency studies of a novel N, O-Multidentate chelating ligand and Its Zr (IV), V (IV), Ru (III), and Cd (II) complexes. *Bioinorg. Chem. Appl.* 2022.

Elganzory, H.H., Hassan, S.S., Aly, S.A., and Abdalla, E.M. (2022b). Synthesis, Characterization, PXRD Studies, Theoretical Calculation, and Antitumor Potency Studies of a Novel N, O-Multidentate Chelating Ligand and Its Zr (IV), V (IV), Ru (III), and Cd (II) Complexes. *Bioinorg. Chem. Appl.* 2022**,** 2006451.

Eswaran, S., Adhikari, A.V., Chowdhury, I.H., Pal, N.K., and Thomas, K. (2010). New quinoline derivatives: Synthesis and investigation of antibacterial and antituberculosis properties. *European journal of medicinal chemistry* 45**,** 3374-3383.

Gaber, M., Fathalla, S.K., and El-Ghamry, H.A. (2019). 2, 4-Dihydroxy-5-[(5-mercapto-1H-1, 2, 4-triazole-3-yl) diazenyl] benzaldehyde acetato, chloro and nitrato Cu (II) complexes: Synthesis, structural characterization, DNA binding and anticancer and antimicrobial activity. *Applied Organometallic Chemistry* 33**,** e4707.

Haghighijoo, Z., Firuzi, O., Hemmateenejad, B., Emami, S., Edraki, N., and Miri, R. (2017). Synthesis and biological evaluation of quinazolinone-based hydrazones with potential use in Alzheimer's disease. *Bioorganic Chemistry* 74**,** 126-133.

Hare, C.R. (1968). *Visible and Ultra Violet Spectroscopy. John Wiley and Sons.* New York, USA: John Wiley and Sons.

Ispir, E. (2009). The synthesis, characterization, electrochemical character, catalytic and antimicrobial activity of novel, azo-containing Schiff bases and their metal complexes. *Dyes and Pigments* 82**,** 13-19.

Katariya, K.D., Shah, S.R., and Reddy, D. (2020). Anticancer, antimicrobial activities of quinoline based hydrazone analogues: synthesis, characterization and molecular docking. *Bioorganic chemistry* 94**,** 103406.

Khan, S.A., Rizwan, K., Shahid, S., Noamaan, M.A., Rasheed, T., and Amjad, H. (2020). Synthesis, DFT, computational exploration of chemical reactivity, molecular docking studies of novel formazan metal complexes and their biological applications. *Applied Organometallic Chemistry* 34**,** e5444.

Kumar, S., Bawa, S., and Gupta, H. (2009). Biological activities of quinoline derivatives. *Mini-Reviews in Medicinal Chemistry* 9**,** 1648.

Liu, Y.-T., Lian, G.-D., Yin, D.-W., and Su, B.-J. (2013). Synthesis, characterization and biological activity of ferrocene-based

Schiff base ligands and their metal (II) complexes. *Spectrochimica Acta Part A: Molecular and Biomolecular Spectroscopy* 100**,** 131-137.

Mandewale, M.C., Patil, U.C., Shedge, S.V., Dappadwad, U.R., and Yamgar, R.S. (2017). A review on quinoline hydrazone derivatives as a new class of potent antitubercular and anticancer agents. *Beni-Suef University journal of basic and applied sciences* 6**,** 354-361.

Manohar, C.S., Manikandan, A., Sridhar, P., Sivakumar, A., Kumar, B.S., and Reddy, S.R. (2018). Drug repurposing of novel quinoline acetohydrazide derivatives as potent COX-2 inhibitors and anti-cancer agents. *Journal of Molecular Structure* 1154**,** 437-444.

Naveen, P., Vijaya Pandiyan, B., Anu, D., Dallemer, F., Kolandaivel, P., and Prabhakaran, R. (2020). A pseudo trinuclear nickel–sodium complex containing tris (8-methyl-2-oxo-quinolidineamino ethylamine): synthesis, spectral characterization, X-ray crystallography and in vitro biological evaluations. *Applied Organometallic Chemistry* 34**,** e5605.

Nunes, D.M., Pessatto, L.R., Mungo, D., Oliveira, R.J., De Campos Pinto, L.M., Da Costa Iemma, M.R., Altei, W.F., Martines, M.a.U., and Duarte, A.P. (2020). New complexes of usnate with lanthanides ions: La (III), Nd (III), Tb (III), Gd (III), synthesis, characterization, and investigation of cytotoxic properties in MCF-7 cells. *Inorganica Chim. Acta* 506**,** 119546.

Özbek, N., Özdemir, Ü.Ö., Altun, A.F., and Şahin, E. (2019). Sulfonamide-derived hydrazone compounds and their Pd (II) complexes: Synthesis, spectroscopic characterization, X-ray structure determination, in vitro antibacterial activity and computational studies. *Journal of Molecular Structure* 1196**,** 707-719.

Parlar, S., Sayar, G., Tarikogullari, A.H., Karadagli, S.S., Alptuzun, V., Erciyas, E., and Holzgrabe, U. (2019). Synthesis, bioactivity and molecular modeling studies on potential anti-Alzheimer piperidinehydrazide-hydrazones. *Bioorganic chemistry* 87**,** 888-900.

Parveen, S., Govindarajan, S., Puschmann, H., and Revathi, R. (2018). Synthesis, crystal structure and biological studies of new hydrazone ligand, 2-(Methoxycarbonyl-hydrazono)-pentanedioic acid and its silver (I) complex. *Inorganica Chimica Acta* 477**,** 66-74.

Pisano, M.B., Kumar, A., Medda, R., Gatto, G., Pal, R., Fais, A., Era, B., Cosentino, S., Uriarte, E., and Santana, L. (2019). Antibacterial activity and molecular docking studies of a selected series of hydroxy-3-arylcoumarins. *Molecules* 24**,** 2815.

Popiołek, Ł., Piątkowska-Chmiel, I., Gawrońska-Grzywacz, M., Biernasiuk, A., Izdebska, M., Herbet, M., Sysa, M., Malm, A., Dudka, J., and Wujec, M. (2018). New hydrazide-hydrazones and 1, 3-thiazolidin-4-ones with 3-hydroxy-2-naphthoic moiety: Synthesis, in vitro and in vivo studies. *Biomedicine & Pharmacotherapy* 103**,** 1337-1347.

Reedijk, J., and Bouwman, E. (1999). *Bioinorganic catalysis*. CRC Press.

Rizk, N.M.H., Aly, S.A., and Khidr, M.A. (2022). Synthesis, characterization, DNA binding of nano Mn2+ and Cu2+ complexes. *Research Journal of Applied Biotechnology* 8**,** 11-26.

Sardaru, M.-C., Marangoci, N.L., Shova, S., and Bejan, D. (2021). Novel Lanthanide (III) Complexes Derived from an Imidazole–Biphenyl–Carboxylate Ligand: Synthesis, Structure and Luminescence Properties. *Molecules* 26**,** 6942.

Sepay, N., and Dey, S.P. (2014). Synthesis and Chemical Reactivity of 4-Oxo-4H-1-benzopyran-3-carboxaldehyde. *Journal of Heterocyclic Chemistry* 51**,** E1-E24.

Yousefi, M., Sedaghat, T., Simpson, J., and Shafiei, M. (2019). Bis-aroylhydrazone based on 2, 2′-bis substituted diphenylamine for synthesis of new

binuclear organotin (IV) complexes: spectroscopic characterization, crystal structures, in vitro DNA-binding, plasmid DNA cleavage, PCR and cytotoxicity against MCF7 cell line. *Applied Organometallic Chemistry* 33**,** e5137.

Zülfikaroğlu, A., Ataol, Ç.Y., Çelikoğlu, E., Çelikoğlu, U., and İdil, Ö. (2020). New Cu (II), Co (III) and Ni (II) metal complexes based on ONO donor tridentate hydrazone: Synthesis, structural characterization, and investigation of some biological properties. *Journal of Molecular Structure* 1199**,** 127012

Table 1. Analytical data of the compounds.

Compounds	Color Yield %	Molecular weight	Conductivity µs	M. W	Found (cal.) %			
					C	H	N	M
Ligand $C_{14}H_{15}N_3OS$	Beige 84	273.35	-	273	61.21 (61.52)	5.52 (5.53)	15.28 (15.37)	-
Cd(II) complex $C_{14}H_{15}CdCl_2\ N_3OS$	Yellow 75	456.67	10	456.67	36.75 (36.82)	3.22 (3.31)	9.11 (9.20)	14.61 (24.62)

Table 2. FT-IR spectral values for H_2L and Cd^{2+} complex.

Compound	ν(N–H)	ν(C=O)	ν(C=N)	ν(C-S)	ν(M-O)	ν(M-N)
Ligand	3410,3096	1705	1612	702	-	-
Cd(II) complex	3402	1571	1600	703	531	453

Table 3. Ground state properties of ligand using B3LYP/6-311G and its Cd(II) complex using B3LYP/LANL2DZ.

Parameter	H_2L	Cd- complex
E_T, Hartree	-1180.10522339	-594.7506
E_{HOMO}, eV	-5.77	-6.48
E_{LUMO}, eV	-1.984	-3.18
ΔE, eV	3.79	3.30
I, eV	5.77	6.48
A,eV	1.98	3.18
χ, eV	3.87	4.83
η, eV	1.89	1.65
S, eV^{-1}	-4.78	-4.89
Dipole Moment (Debye)	6.67	19.4007

Table 4. Some of the optimized bond length, Å and bond angles, degrees, H_2L ligand using B3LYP/6-311G(++)d,p and its Cd(II) complex using B3LYP/LANL2DZ.

Bond length (Aº)	H_2L	Cd-complex	Bond angles (Deg.)	H_2L	Pd- CTPTA
R(C1-C2)	1.533	1.530	**A(C2-C1-O3)**	120.919	121.473
R(C1-O3)	1.238	1.263	**A(O3-C1-N4)**	125.455	122.925
R(C1-N4)	1.380	1.368	**A(C1-N4-N5)**	120.394	118.867
R(N4-N5)	1.377	1.392	**A(N4-N5-C6)**	119.743	120.104
R(C2-12N)	1.460	1.460	**A(O3-Cl21-Cl22)**	---	52.814
R(Cd-Cl21)	---	2.448	**A(O3-Cd-N5)**	---	68.771
			A(Cl22-Cd-N5)	---	106.365

Table 5. The *in-vitro* antibacterial activity:

Sample / Pathogenic microorganism	H_2L	Cd(II) complex	Control
Bacillus subtilis (ATCC 6633)	26±0.1	30±0.1	28±0.1
Staph.aureus (ATCC 6538)	23±0.1	25±0.2	24±0.3
Escherichia coli (ATCC 8739)	28±0.2	31±0.1	23±0.2
P. aeruginosa (ATCC 90274)	21±0.2	22±0.1	18±0.1

6. The results of IC_{50} values of the ligand and Cd(II) complex against **MCF7** Cell line

Compound	MCF7 Cell line (IC_{50} values) (µg/ml)
Cisplatine	28.36
H_2L	54.15
Cd(II) Complex	43.12

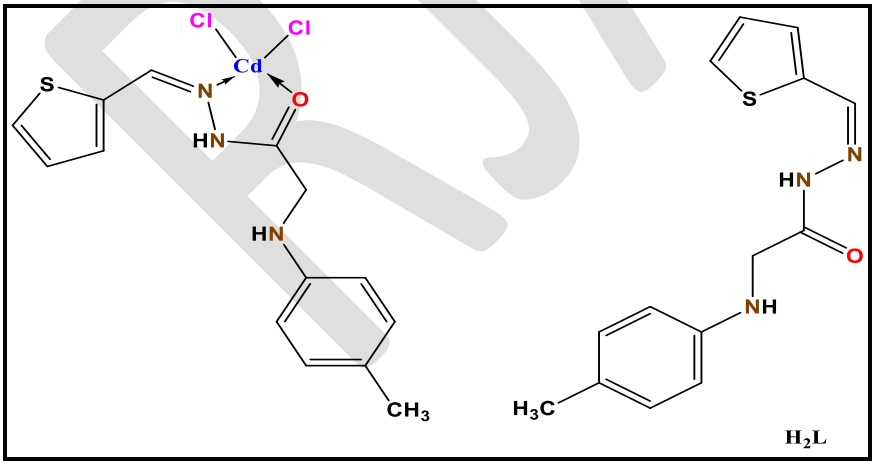

Structures 1. Proposed structures of ligand and Cd (II) complex.

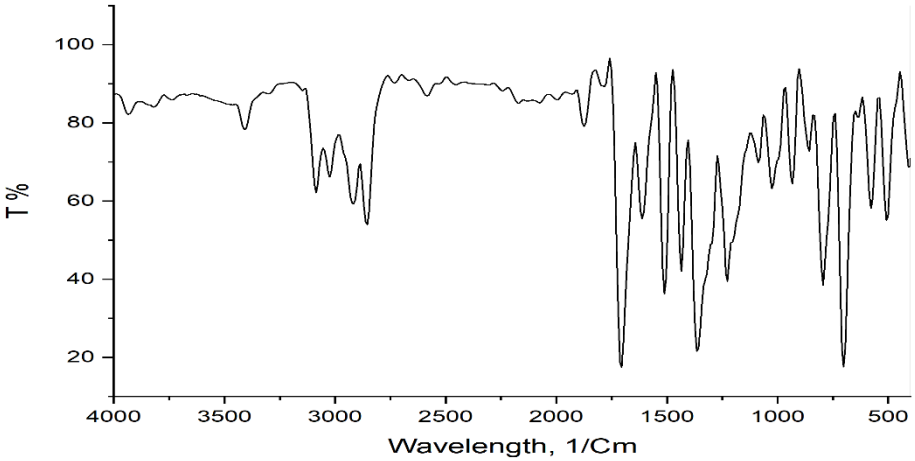

Figure1 FT-IR spectrum of ligand

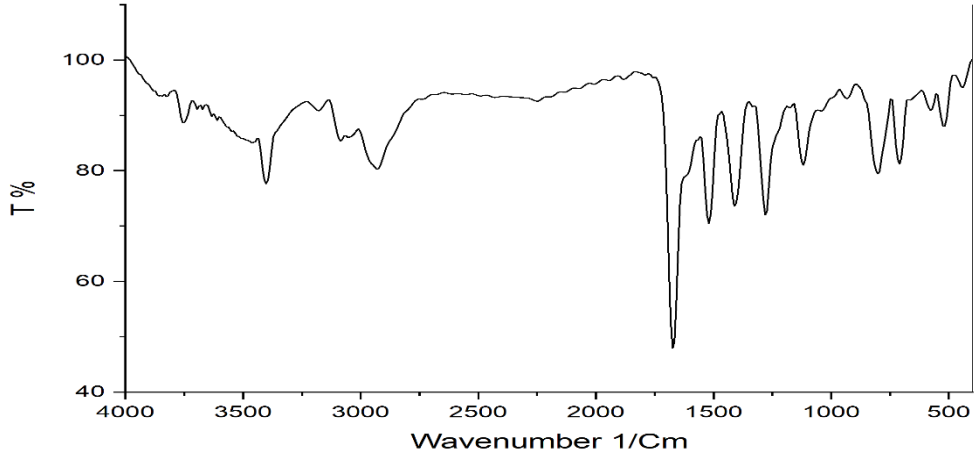

Figure 2 FT-IR spectrum of Cd^{2+} complex

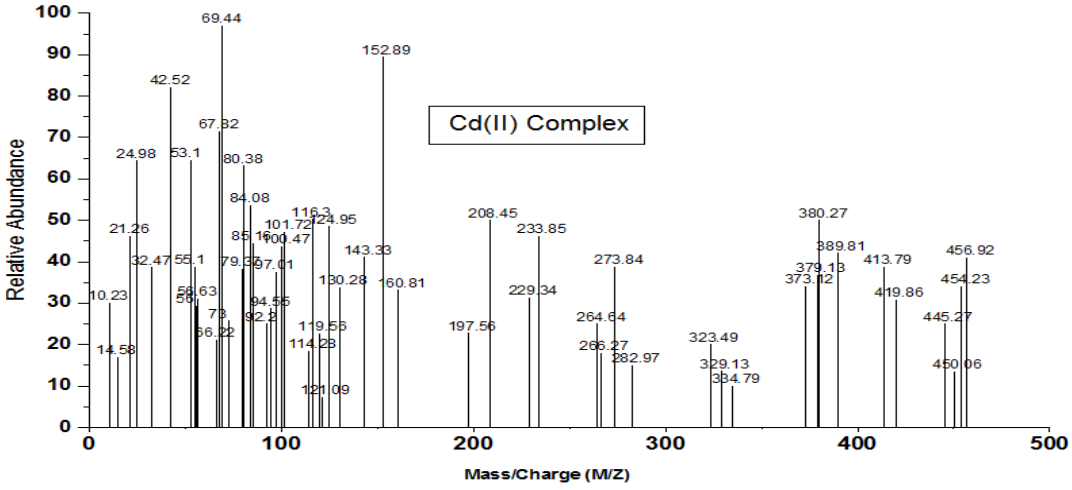

Figure 3. Mass spectra of ligand and Cd^{2+} complex

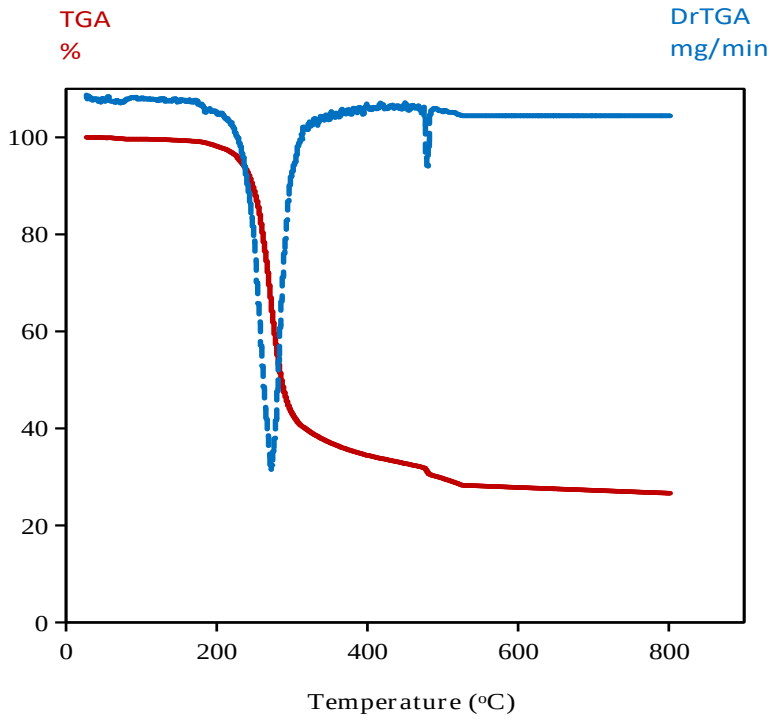

Figure 4. TGA curve of Cd(II) complex.

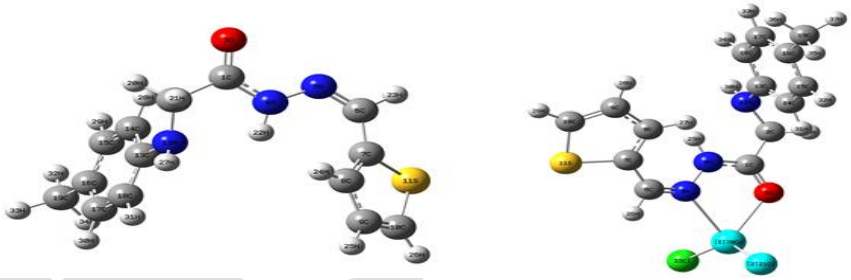

Figure 5. Optimization geometry of H_2L and Cd^{2+} complex, respectively.

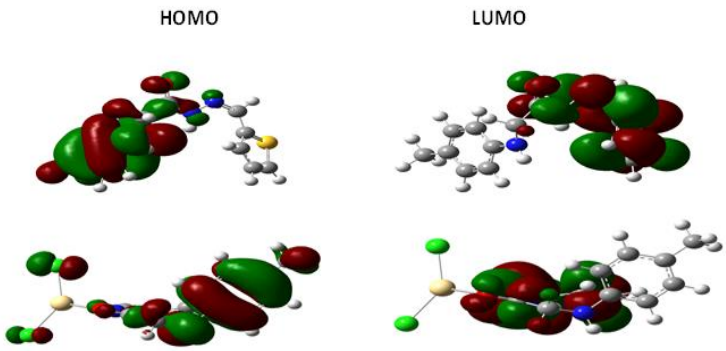

Figure 6. Molecular graphs of H_2L and Cd^{2+} complex

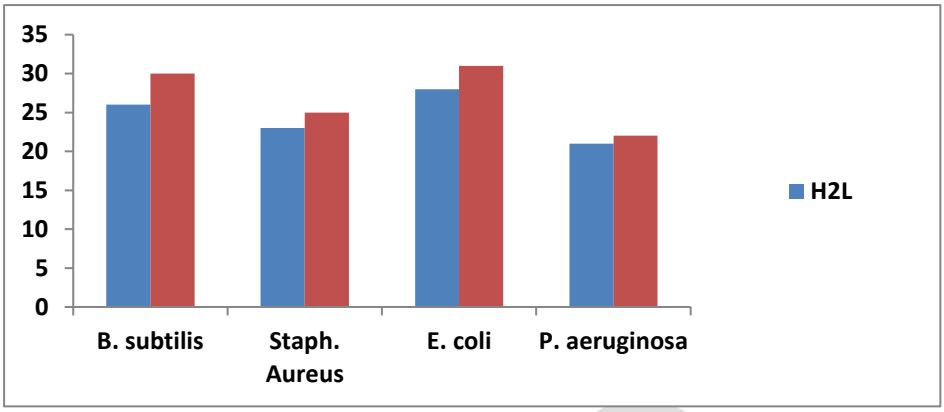

Figure 7: the antibacterial activity of Cd(II) complex and ligand at a concentration of 10 mg ml $^{-1}$ in relation to gentamycin and ampicillin as standard medications

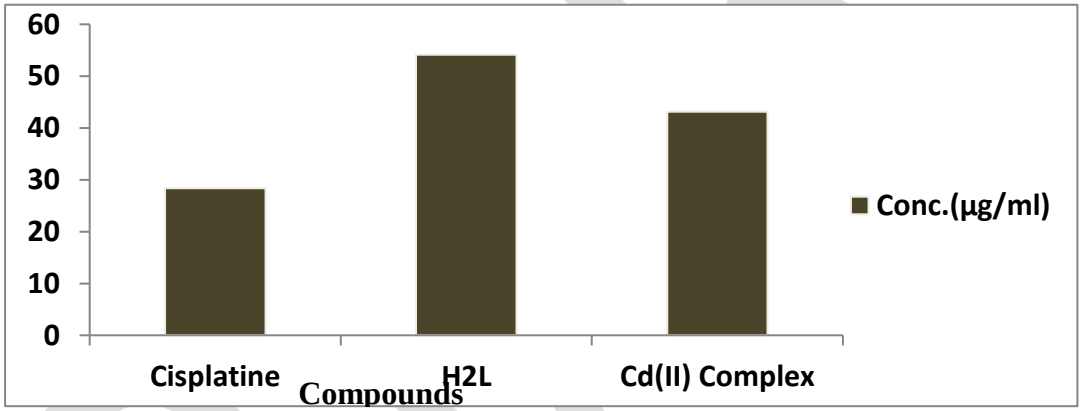

Figure 8. IC_{50} values of Cd (II) complex and ligand against MCF7 cancer cell line in comparison to cisplatin.

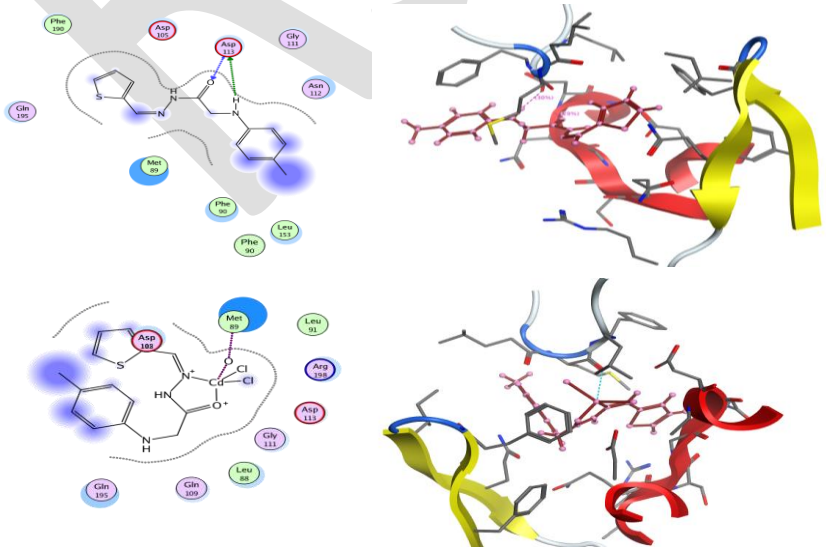

Figure 9: 2D and 3D Diagrams of the interaction between Ligand and Cd(II) complex with Penicillin-binding protein PBP enzyme.